Journal of Power Sources 261 (2014) 136–140

Contents lists available at ScienceDirect

Journal of Power Sources

journal homepage: www.elsevier.com/locate/jpowsour

Short communication

Oxygen vacancy induced carbon deposition at the triple phase boundary of the nickel/yttrium-stabilized zirconia (YSZ) interface

Yanxing Zhang, Zhaoming Fu, Mingyang Wang, Zongxian Yang*

College of Physics and Electronic Engineering, Henan Normal University, Xinxiang, Henan 453007, People's Republic of China

HIGHLIGHTS

- The carbon deposition at the Ni/YSZ interface with O vacancy is studied.
- The adsorption and diffusion properties of CH on the Ni/YSZ are studied.
- The CH can easily diffuse and be trapped at the interface O vacancy.
- The CH can dissociate to C and H atom easily at the interface O vacancy.

GRAPHICAL ABSTRACT

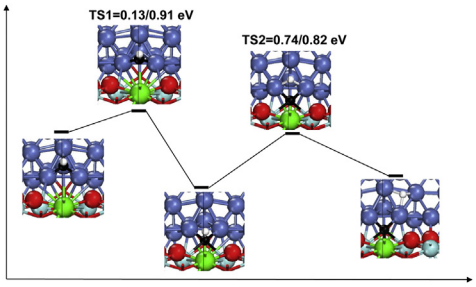

ARTICLE INFO

Article history:
Received 8 January 2014
Received in revised form
14 March 2014
Accepted 17 March 2014
Available online 25 March 2014

Keywords:
Solid oxide fuel cell
Carbon deposition
Nickel/yttrium-stabilized zirconia anode
Oxygen vacancy
Triple phase boundary (TPB)

ABSTRACT

The carbon deposition at the Triple Phase Boundary (TPB) of the Nickel/Yttrium-Stabilized Zirconia (YSZ) interface is studied using the first-principles method based on density functional theory, with consideration of the interface oxygen vacancy. It is found that the CH fragment (the most stable dissociation products of CH_4 on Ni catalyst) can easily diffuse and be trapped at the O vacancy. The trapped CH can dissociate to C and H with a much lower dissociation barrier (0.74 eV) as compared with that (1.39 eV) on the pure Ni (111) surface. Therefore, we propose that the carbon deposition may form easily at the interface oxygen vacancy of TPB as compared with that on the pure Ni (111) surface, which offers new understanding on the carbon deposition of the Ni/YSZ anode of solid oxide fuel cell.

1. Introduction

Solid oxide fuel cells (SOFCs) are expected to be a crucial technology in the future power generation [1,2]. SOFCs offer many desirable advantages compared to other types of fuel cells and conversion devices due to the use of solid electrolytes, lack of moving parts, ability to circumvent precious metal use, high efficiency, low pollution, and fuel flexibility. The fuel flexibility is achieved by reducing the oxygen molecules in the cathode compartment and transporting the oxygen ions for fuel oxidation through the solid state electrolyte, which requires high operating temperatures (600–1000 °C). Unfortunately, the high operating temperatures of SOFC lead to a number of complications that can be detrimental for the cell performance. These include low anode stability to redox cycling [3,4], adverse reactions between adjacent cell components [5,6], and temperature gradients in the cell parts occurring during the start-up and shut-down phase [7,8]. Moreover, the direct electrochemical oxidation of hydrocarbon fuels in SOFCs is, in principle, possible, but has resulted in carbon

* Corresponding author.
E-mail addresses: yzx@henannu.edu.cn, zongxian.yang@163.com, yzx@htu.cn (Z. Yang).

http://dx.doi.org/10.1016/j.jpowsour.2014.03.056
0378-7753/

deposition (coke formation) at elevated temperatures (most severely at $T > 800$ °C), which results in chemical deactivation of the anode [9]. The formation of coke over nickel-based catalysts during the partial oxidation or the steam and CO_2 reforming of methane or other hydrocarbons has been extensively investigated during the past decades [10–12]. Coke accumulation has been suggested to be a balance between the formation and the removal of coke which determines the degree of coking [13]. The growth of carbon on the nickel surface during a hydrocarbon reforming process has been explored experimentally in detail by Sehested [14]. Three types of carbon have been observed in a reformer: pyrolytic, encapsulating, and whisker carbons. Ni catalyzes the formation of carbon deposition at the anode of SOFCs under reducing condition [15,16], which would block the active sites and deactivate the Ni catalysts, ultimately destroy the catalyst completely [16–20]. Coke formation on nickel surfaces has been fairly well investigated. The carbon growth on the Ni catalysts is also generally accepted to occur via the dissolution–precipitation mechanism [21–23]. For example, methane (CH_4) adsorbs onto the nickel surface and then decomposes into C and H; later, the carbon atoms dissolve into the bulk of the Ni particles, diffuse through the Ni particles, and finally precipitate as carbon at their rear side. Though it is true that Ni generally catalyzes carbon deposition as well as reforming reactions, it also depends on many different parameters such as temperature, Ni/YSZ formulation, use of additives and steam to-carbon ratio [24–26]. Steam reforming of hydrocarbons involves a risk of carbon deposition. The probability for carbon depositions depends on the steam-to-carbon ratio and on the catalytic composition [27,28]. The risk of carbon deposition can be decreased if the pre-reforming is carried out before the cell, or the anode structure or configuration is modified. More detailed introductions to the carbon deposition studies are shown in several excellent review papers [14,25,29–31].

In general, researchers [32–34] studied the carbon formation started at the dissociation of CH_4 on the Ni (111) surface. The successive dehydrogenations of CH_4 to CH_3, CH_2, CH are favorable on Ni (111) with the activation barriers less than 1 eV (0.91, 0.67, 0.30 eV), while the barrier of last step of dehydrogenation of CH is as large as 1.36 [32], 1.39 [33] eV with endothermic reaction energies of 0.54 [34] and 0.49 [32] eV. Most of the theoretical studies of methane adsorption and dissociation on Ni catalysts arrived at conclusions that the CH species has the most thermodynamic stability [35–37] among the dissociation species (CH_x ($x = 0$–3)) of CH_4. For example, DFT results of Nikolla and coworkers [36] on the reaction energies for various elementary steps involved in methane stream reforming on Ni(111) showed that the CH fragment is the most adsorbate species on Ni(111) surface. As known, the anode of SOFC is the Ni/YSZ composite, instead of the Ni itself. The ideal Ni(111) only represents the anode region beyond the TPB. It is generally believed that the active sites of the Ni/YSZ anode are covered with deposited carbon, resulting in the deactivation, loss of cell performance and lower SOFC reliability [15,26,38,39]. Shishkin and Ziegler's studies [40,41] on hydrogen oxidation at the Ni/YSZ interface indicated that the most active sites are located at the Ni/YSZ interface. Our previous works [42,43] showed that the sulfur atom would be strongly adsorbed at the vacancy site at the Ni/YSZ interface and is more favorable than that on a Ni surface. These findings all indicate that the vacancy site at the Ni/YSZ interface is highly active compared with the ideal Ni (111) surface beyond the TPB region. Recently, Shishkin and Ziegler [44] studied the carbon removal from the anode triple-phase boundary (TPB) of SOFCs by adsorbed water molecules. They found that the formation of interfacial carbon (at the O vacancy site) is more favorable than that on a Ni surface, indicating that the TPB of Ni/YSZ can also be clogged by carbon atoms. Ihara et al. have also studied [45] the deposited pyrolytic carbon at the three-phase boundary in experiments. However, the studies on the carbon deposition at the TPB of the Ni/YSZ interface, especially for that with O vacancy, are very scarce.

In this work, the processes of CH diffusion to the vacancy site at the Ni/YSZ interface and the dehydrogenation of CH at the vacancy site are studied. It is found that the CH can dissociate easily at the vacancy site with a much lower barrier (0.74 eV) as compared with that (1.39 [33], 1.36 [32] eV) at the Ni (111) surface.

2. Model and computation method

All calculations presented in this work are performed employing the periodic density functional theory (DFT) method implemented in the Vienna Ab-Initio Simulation Package (VASP) [46]. The exchange–correlation interactions are treated with the Perdew–Burke–Ernzerhof (PBE) functional [47]. Spin-polarized calculations are applied throughout. The electron-ion interactions are treated using the projector augmented wave (PAW) method [48,49]. The wave functions are expanded in plane waves with a cut off energy of 408 eV. The TPB model of the Ni/YSZ cermet used in the Shishkin and Ziegler's work [40] is adopted as the substrate, where the YSZ slab has the horizontal dimensions of 12.56 × 7.25 Å. In the proposed structure, both Ni and YSZ face each other by the (111) crystallographic planes, with a small lattice mismatch of 3% in the direction with sustained translational symmetry. Experimentally, Abe et al. [50] and other researchers [51,52] fabricated and characterized the Ni/YSZ anode cermet, which has the structure with the (111) planes of the Ni part parallel to the (111) planes of YSZ. Using the transmission electron microscopy technique (TEM), they have shown a clear absence of amorphous phases at the interface with a (111)//(111) orientation relationship between Ni and YSZ. A vacuum layer of 15 Å is used to separate the periodic images in the direction perpendicular to the surface. The Monkhorst–Pack k-point mesh of 2 × 3 × 1 is used for the Brillouin zone (BZ) sampling. The atoms in the bottom multilayer are kept fixed for all calculations. Structural optimization of all systems is performed until the atomic forces drop below 0.02 eV $Å^{-1}$. The climbing image nudged elastic band (CI-NEB) [53] method is employed to calculate the transition states and migration barriers. The adsorption energy of an atom or molecular fragment (e.g., C or CH) is defined by

$$E_{ads} = E_{CH\ or\ C} + E_{Ni/YSZ-Ov} - E_{CH\ or\ C-Ni/YSZ-Ov} \quad (1)$$

where $E_{CH\ or\ C}$ is the energy of a single CH fragment or a C atom simulated in the 8 × 8 × 8 Å box; $E_{CH\ or\ C-Ni/YSZ-Ov}$ and $E_{Ni/YSZ-Ov}$ are the total energies of the Ni/YSZ with an interface oxygen vacancy (Ni/YSZ-Ov) with and without the CH or C adsorbate, respectively. The $1s^2$ of H, $2s^22p^2$ of C, $2s^22p^4$ of O, $3d^84s^2$ of Ni, $4s^24p^65s^24d^2$ of Zr and $4s^24p^65s^24d^1$ of Y are treated as valence electrons in the DFT calculations. The Bader charge [54] analysis scheme is applied to determine the atomic charges and charge transfer. Pure GGA functionals underestimate the band gap and, as a consequence, may affect the other properties. This drawback can be remedied in higher levels of theory, e.g., the weighted density approximation (WDA), screened exchange (sX) [55], GW approximation [56], and hybrid functionals (HSE06, PBE0, B3LYP) [57,58], etc. However, these methods demand greater computational effort and are not always feasible for large models and extensive sampling. For this reason, in our work we apply the GGA approximation, which is known to give good energetics, and the qualitative description of the electronic structure. We tried to use the international system of units (SI) in this paper. However, we keep some of the popular units used the micro world and give their equivalent in SI for clarity, e.g.,

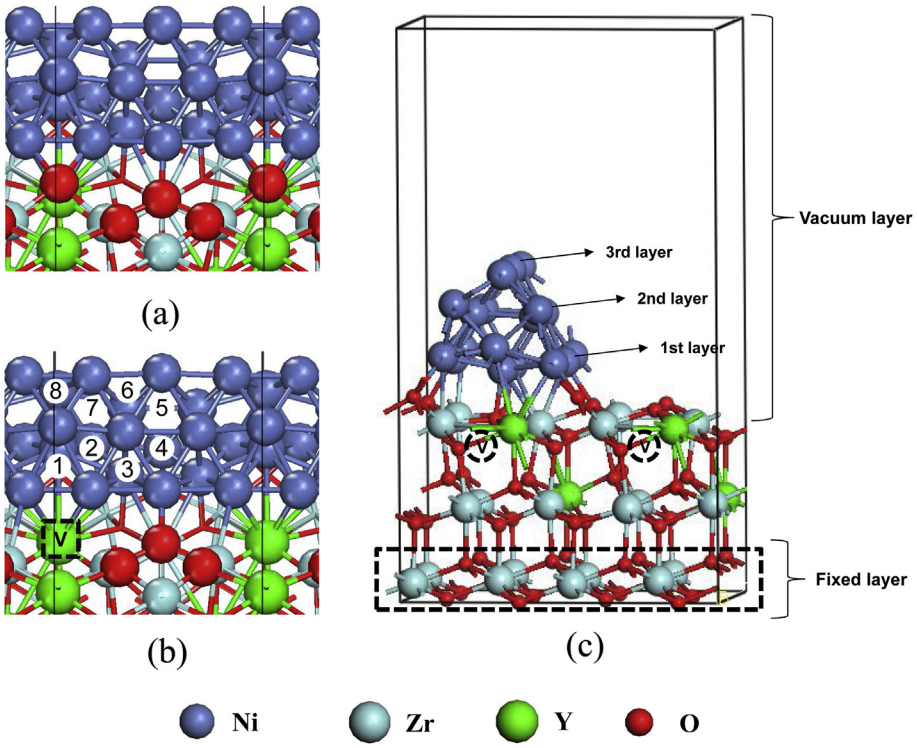

Fig. 1. The Ni/YSZ model: (a), (b) right views, and (c) side views, black dash square in (b) represents the oxygen vacancy at the Ni/YSZ interface, black dash circles in (c) represent the intrinsic oxygen vacancies in the YSZ lattice.

1 eV = 1.60217733 × 10^{-19} J; 1 Å = 10^{-10} m; 1 e = 1.60217733 × 10^{-19} C.

3. Results and discussions

3.1. The adsorption and diffusion of CH at the Ni/YSZ-Ov interface

Our TPB model of the Ni/YSZ system contains three Ni layers on YSZ as shown in Fig. 1. Since oxygen vacancy usually exists after the hydrogen oxidation at the Ni/YSZ interface, we consider the adsorption and diffusion of CH at the Ni/YSZ-Ov interface. For the Ni/YSZ-Ov system, there is a significant charge transfer of 0.96 electrons from the YSZ-Ov support to the Ni part as compared with that in Ni/YSZ based on the Bader charge analysis [54]. The possible CH adsorption sites are shown in Fig. 1(c) and the data of adsorption properties are shown in Table 1. It is found that the adsorption energy and excess charges of CH at the Ni part of the Ni/YSZ-Ov system are in the range of 6.23–6.58 eV and 0.53–0.66 e, respectively, which are close to the values (6.41 eV, 0.36 e) of CH on the Ni(111) surface [32]. In contrast, the most stable CH adsorption is at the vacancy site, in which the adsorption energy is as large as 7.36 eV and the CH gets more electrons (~1.23 e), which is close to the value of the sulfur atom at the vacancy site [42].

We suppose that the CH diffusion to the vacancy site experiences a two-step process: 1) the CH diffuses on the ideal Ni (111) surface beyond the TPB region; 2) the CH diffuses from the Ni part at the TPB region to the vacancy site. It is known that the CH diffusion on the ideal Ni (111) surface is quite easy (with a diffusion barrier of 0.35 eV [32] from the HCP site to the FCC site), we focus on the second process and calculate the diffusion barrier of CH from the most stable adsorption site 1 to the vacancy site.

Table 1
The adsorption properties of CH on the Ni/YSZ-Ov, including the adsorption energy (E_{ads}, in eV), the bond length of the C–Ni(Zr) ($d_{C-Ni(Zr)}$, in Å) and C–H (d_{C-H}, in Å), the excess number of electrons of the adsorbed CH, CH-Chg (in *e*).

Ni/YSZ-Ov	E_{ads}	d_{C-Ni} (d_{C-Zr})	d_{C-H}	CH-Chg
1	6.58	1.82, 1.82, 1.90	1.10	0.67
2	6.41	1.83, 1.83, 1.86	1.10	0.62
3	6.28	1.81, 1.83, 1.91	1.10	0.62
4	6.38	1.82, 1.82, 1.84	1.10	0.53
5	6.26	1.82, 1.83, 1.84	1.10	0.58
6	6.23	1.82, 1.84, 1.87	1.10	0.60
7	6.27	1.82, 1.84, 1.85	1.10	0.61
8	6.30	1.83, 1.83, 1.84	1.10	0.62
Vac	7.36	1.91, 1.92 (2.36, 2.36)	1.13	1.23

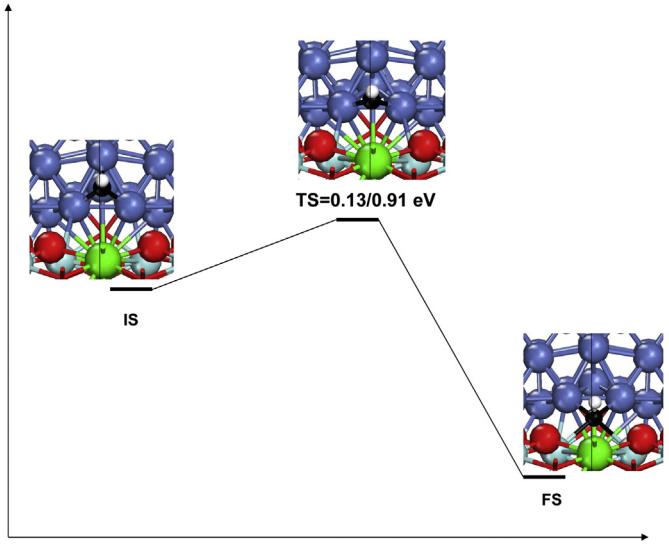

Fig. 2. The minimum energy path (MEP) for the diffusion of CH fragment.

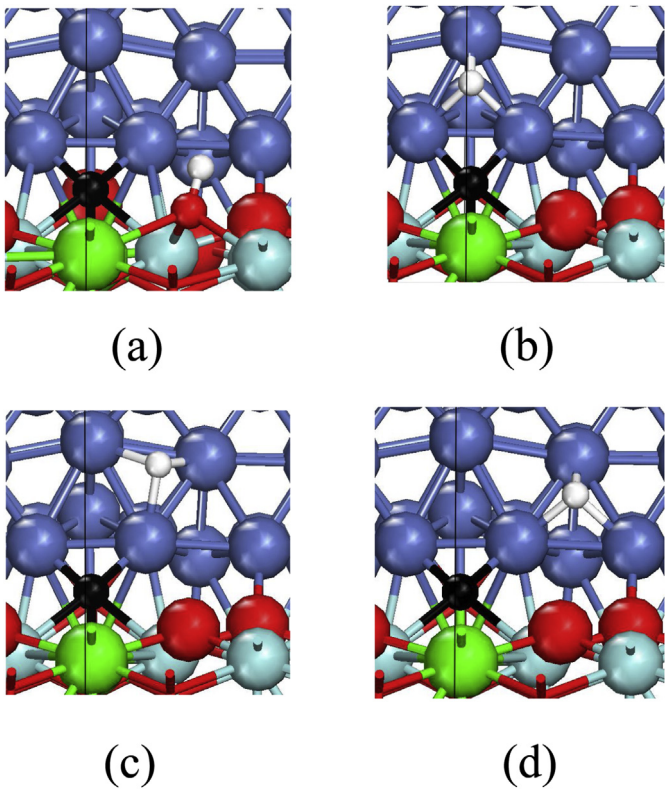

Fig. 3. The final states for the CH fragment dissociation.

The minimum energy path (MEP) for the diffusion of CH from site 1 to the vacancy site is shown in Fig. 2. The diffusion barrier is only 0.13 eV with the reverse barrier as large as 0.91 eV. So the two processes all have very small barriers (0.35, 0.13 eV), indicating that the CH fragment can diffuse easily to the vacancy site. The large reverse barrier (0.91 eV) means that the CH fragment would be trapped at the vacancy site.

3.2. The dehydrogenation of CH at the vacancy site of the Ni/YSZ-Ov

Now, we study the dehydrogenation of CH at the vacancy site of the Ni/YSZ-Ov, which is taken as the initial state (IS). The converged dissociation configurations are shown in Fig. 3. It is found the H atom is not favorable at the O top site at the interface as shown in Fig. 3(a), which has a quite large endothermic energy (0.65 eV) compared with the energy of CH at the vacancy site of the TPB, while the H atom at the Ni surface is relatively more favorable when it is away from the interface. The energies of configurations shown in Fig. 3(b)–(d) are (endothermic) higher in energy by 0.51, 0.12, 0.09 eV compared with the energy of CH at the vacancy site. The CH dissociation energy profile is shown in Fig. 4 if the structures in Fig. 3(a)–(d) are taken as the final states (FS1, FS2, FS3, FS4), respectively. It is found that the dissociation of CH with the formation of OH at the O site is difficult with a dissociation barrier of as high as 2.06 eV (as shown in the transition state of TS1), while the dissociation paths with the final states as shown in Fig. 3(b)–(d) all have smaller barriers (0.74, 0.74, 0.83 eV) as shown in the transition states of TS2, TS3 and TS4. The TS2 and TS3 have the same geometry configuration. It is found that for the process from IS to FS3, the dehydrogenation of CH is not only less endothermic with smaller reaction energy (0.12 eV), but also has a much smaller dissociation barrier (0.74 eV) as compared with those (0.54, 1.39 eV) on the Ni(111) surface (e.g., the region beyond the TPB region).

4. Discussion

It is found that CH would easily diffuse to the vacancy site at the Ni/YSZ-Ov interface and the dehydrogenation barrier (0.74 eV) of the CH at the vacancy site is lower by 0.65 eV as compared with that

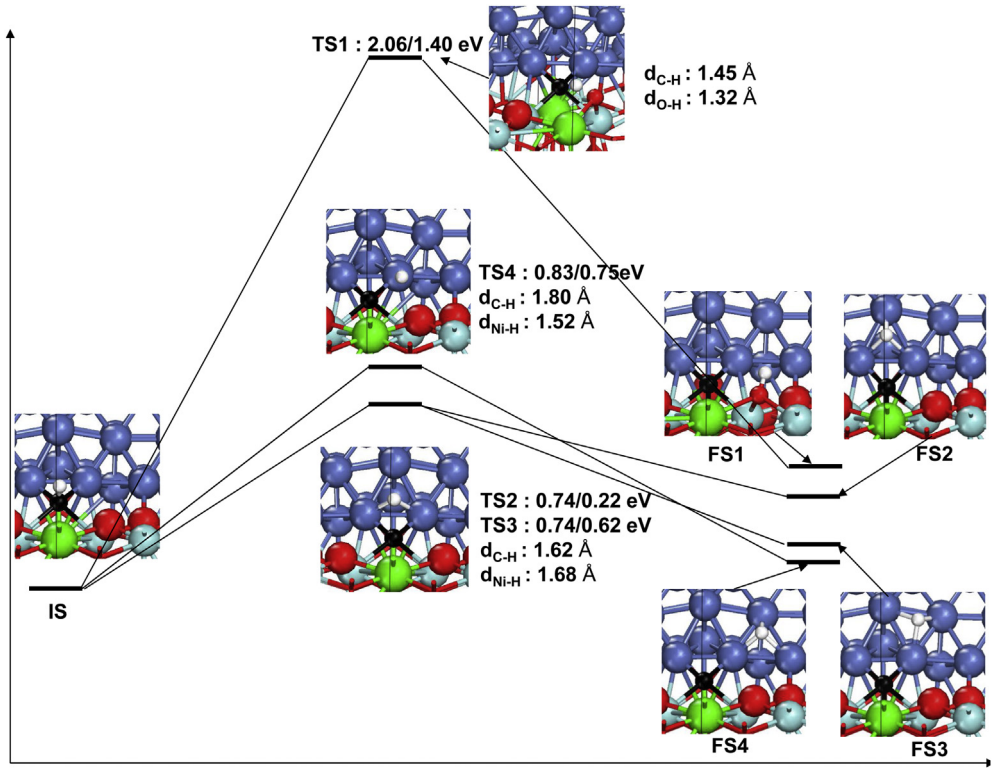

Fig. 4. The MEPs for the different dissociation paths of the CH fragment.

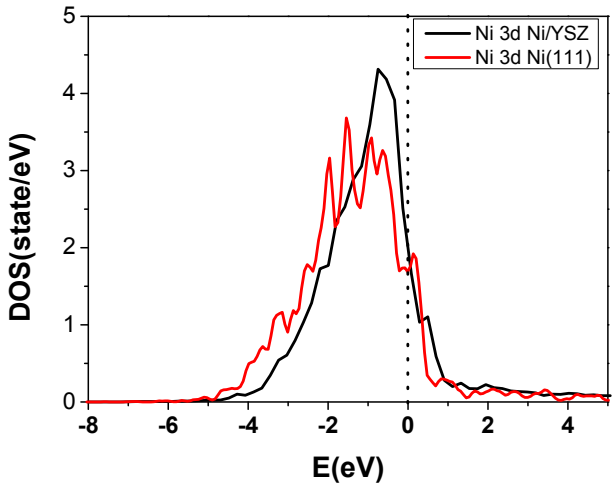

Fig. 5. The density of states (DOS) of Ni 3d at the Ni/YSZ-Ov vacancy site and on the Ni (111) surface (the vertical dash line represents the Fermi level).

(1.39 eV) on the Ni (111) surface. The density of states (DOS) of Ni 3d at vacancy site of Ni/YSZ and that on the Ni(111) surface are shown in Fig. 5, which shows that the Ni 3d DOS near the Fermi level is much higher at the Ni/YSZ vacancy site than that on the Ni (111) surface. The calculated d-band center of the Ni atom at the vacancy site is much shallower than that on the Ni (111) surface (−1.43 *vs* −1.66 eV). The lower coordination number (6) and the more excess electrons (0.46 e) of the Ni atom at the vacancy site as compared with those (9, 0.02 e) on the Ni (111) surface make the Ni atom at the vacancy site have shallower d band-center and higher activity for the dissociation of CH. The high active Ni atom at the vacancy site contributes the lower dissociation barrier of CH (0.74, 0.83 eV *vs* 1.39 eV), which might be the mechanism for the carbon deposition at the TPB of the Ni/YSZ anode.

5. Conclusion

In this work, the carbon deposition at the TPB of the Ni/YSZ-Ov system is studied using the first-principles method based on density functional theory. It is found that the CH fragment (the most stable dissociation product of CH_4 on Ni catalyst) can easily diffuse and be trapped at interface O vacancy site. The trapped CH can dissociate to C and H atoms with lower dissociation barrier (0.74 eV) as compared as that (1.39 eV) on the pure Ni (111) surface. Therefore the interface oxygen vacancy may induce the formation of carbon deposition at the TPB of the Ni/YSZ anode. This work sheds new lights on the mechanism on the carbon deposition of the Ni/YSZ anode.

Acknowledgments

This work was supported by the National Natural Science Foundation of China (Grant Nos. 11174070 and 11247012) and the Innovation Scientists and Technicians Troop Construction Projects of Henan Province, China (Grant No. 104200510014).

References

[1] R.M. Ormerod, Chem. Soc. Rev. 32 (2003) 17–28.
[2] M.C. Williams, J.P. Strakey, W.A. Surdoval, L.C. Wilson, Solid State Ionics 177 (2006) 2039–2044.
[3] D. Sarantaridis, A. Atkinson, Fuel Cells 7 (2007) 246–258.
[4] M. Pihlatie, A. Kaiser, P.H. Larsen, M. Mogensen, J. Electrochem. Soc. 156 (2009) B322–B329.
[5] S.P. Simner, J.P. Shelton, M.D. Anderson, J.W. Stevenson, Solid State Ionics 161 (2003) 11–18.
[6] R. Maric, J. Roller, R. Neagu, J. Therm. Spray Technol. 20 (2011) 696–718.
[7] W. Bujalski, C.M. Dikwal, K. Kendall, J. Power Sources 171 (2007) 96–100.
[8] A. Mirahmadi, K. Valefi, J. Fuel Cell Sci. Technol. 8 (2011).
[9] E.P. Murray, T. Tsai, S. Barnett, Nature 400 (1999) 649–651.
[10] O. Yamazaki, K. Tomishige, K. Fujimoto, Appl. Catal. A 136 (1996) 49–56.
[11] K. Tomishige, Y.-G. Chen, K. Fujimoto, J. Catal. 181 (1999) 91–103.
[12] J. Luo, Z. Yu, C. Ng, C. Au, J. Catal. 194 (2000) 198–210.
[13] D. Trimm, Catal. Today 49 (1999) 3–10.
[14] J. Sehested, Catal. Today 111 (2006) 103–110.
[15] C.M. Finnerty, N.J. Coe, R.H. Cunningham, R.M. Ormerod, Catal. Today 46 (1998) 137–145.
[16] H.S. Bengaard, J.K. Nørskov, J. Sehested, B. Clausen, L. Nielsen, A. Molenbroek, J. Rostrup-Nielsen, J. Catal. 209 (2002) 365–384.
[17] J.R. Rostrup-Nielsen, J. Catal. 85 (1984) 31–43.
[18] H. Timmermann, D. Fouquet, A. Weber, E. Ivers-Tiffee, U. Hennings, R. Reimert, Fuel Cells 6 (2006) 307–313.
[19] F. Abild-Pedersen, J.K. Nørskov, J.R. Rostrup-Nielsen, J. Sehested, S. Helveg, Phys. Rev. B 73 (2006) 115419.
[20] S. Helveg, C. López-Cartes, J. Sehested, P.L. Hansen, B.S. Clausen, J.R. Rostrup-Nielsen, F. Abild-Pedersen, J.K. Nørskov, Nature 427 (2004) 426–429.
[21] J. Rostrup-Nielsen, D.L. Trimm, J. Catal. 48 (1977) 155–165.
[22] A. Kock, P. De Bokx, E. Boellaard, W. Klop, J.W. Geus, J. Catal. 96 (1985) 468–480.
[23] W.L. Holstein, J. Catal. 152 (1995) 42–51.
[24] M. Andersson, H. Paradis, J. Yuan, B. Sundén, J. Fuel Cell Sci. Technol. 8 (2011) 031013.
[25] M. Andersson, H. Paradis, J. Yuan, B. Sundén, Int. J. Energy Res. 35 (2011) 1340–1350.
[26] J.-H. Koh, Y.-S. Yoo, J.-W. Park, H.C. Lim, Solid State Ionics 149 (2002) 157–166.
[27] S.H. Clarke, A.L. Dicks, K. Pointon, T.A. Smith, A. Swann, Catal. Today 38 (1997) 411–423.
[28] M.D. Gross, J.M. Vohs, R.J. Gorte, Electrochim. Acta 52 (2007) 1951–1957.
[29] K. Girona, J. Laurencin, J. Fouletier, F. Lefebvre-Joud, J. Power Sources 210 (2012) 381–391.
[30] S. McIntosh, R.J. Gorte, Chem. Rev. 104 (2004) 4845–4866.
[31] W. Wang, C. Su, Y. Wu, R. Ran, Z. Shao, Chem. Rev. 113 (2013) 8104–8151.
[32] M. Wang, Z. Fu, Z. Yang, Phys. Lett. A 377 (2013) 2189–2194.
[33] C. Fan, Y.-A. Zhu, Y. Xu, Y. Zhou, X.-G. Zhou, D. Chen, J. Chem. Phys. 137 (2012) 014703.
[34] D.W. Blaylock, T. Ogura, W.H. Green, G.J. Beran, J. Phys. Chem. C 113 (2009) 4898–4908.
[35] E. Nikolla, J. Schwank, S. Linic, J. Catal. 250 (2007) 85–93.
[36] E. Nikolla, J.W. Schwank, S. Linic, Catal. Today 136 (2008) 243–248.
[37] N.M. Galea, D. Knapp, T. Ziegler, J. Catal. 247 (2007) 20–33.
[38] A.L. Dicks, J. Power Sources 61 (1996) 113–124.
[39] T. Takeguchi, Y. Kani, T. Yano, R. Kikuchi, K. Eguchi, K. Tsujimoto, Y. Uchida, A. Ueno, K. Omoshiki, M. Aizawa, J. Power Sources 112 (2002) 588–595.
[40] M. Shishkin, T. Ziegler, J. Phys. Chem. C 113 (2009) 21667–21678.
[41] M. Shishkin, T. Ziegler, J. Phys. Chem. C 114 (2010) 11209–11214.
[42] Y. Zhang, Z. Lu, Z. Yang, T. Woo, J. Power Sources 237 (2013) 128–131.
[43] Y. Zhang, Z. Fu, S. Dong, Z. Yang, Phys. Chem. Chem. Phys. 16 (2014) 1033–1040.
[44] M. Shishkin, T. Ziegler, J. Phys. Chem. C 117 (2013) 7086–7096.
[45] M. Ihara, K. Matsuda, H. Sato, C. Yokoyama, Solid State Ionics 175 (2004) 51–54.
[46] G. Kresse, J. Furthmüller, Phys. Rev. B 54 (1996) 11169.
[47] J.P. Perdew, K. Burke, M. Ernzerhof, Phys. Rev. Lett. 77 (1996) 3865–3868.
[48] P.E. Blöchl, Phys. Rev. B 50 (1994) 17953.
[49] G. Kresse, D. Joubert, Phys. Rev. B 59 (1999) 1758.
[50] H. Abe, K. Murata, T. Fukui, W.J. Moon, K. Kaneko, M. Naito, Thin Solid Films 496 (2006) 49–52.
[51] M.C. Muñoz, S. Gallego, J.I. Beltrán, J. Cerdá, Surf. Sci. Rep. 61 (2006) 303–344.
[52] T. Sasaki, K. Matsunaga, H. Ohta, H. Hosono, T. Yamamoto, Y. Ikuhara, Mater. Trans. 45 (2004) 2137–2143.
[53] G. Henkelman, B.P. Uberuaga, H. Jónsson, J. Chem. Phys. 113 (2000) 9901.
[54] G. Henkelman, A. Arnaldsson, H. Jónsson, Comput. Mater. Sci. 36 (2006) 354–360.
[55] K. Xiong, J. Robertson, M. Gibson, S. Clark, Appl. Phys. Lett. 87 (2005) 183505.
[56] B. Králik, E.K. Chang, S.G. Louie, Phys. Rev. B 57 (1998) 7027.
[57] A. Alkauskas, P. Broqvist, F. Devynck, A. Pasquarello, Phys. Rev. Lett. 101 (2008) 106802.
[58] P. Broqvist, A. Pasquarello, Appl. Phys. Lett. 89 (2006) 262904.